

# Simultaneous Generation of Arbitrary Assembly of Polarization States with Geometrical-Scaling-Induced Phase Modulation

Ya-Jun Gao,<sup>1</sup> Xiang Xiong,<sup>1</sup> Zhenghan Wang,<sup>1</sup> Fei Chen,<sup>1</sup> Ru-Wen Peng,<sup>1,\*</sup> and Mu Wang<sup>1,†</sup>

<sup>1</sup>*National Laboratory of Solid State Microstructures, School of Physics,  
and Collaborative Innovation Center of Advanced Microstructures, Nanjing University, Nanjing 210093, China*

Manipulating the polarization of light on the micro/nano scale is essential for integrated photonics and quantum optical devices. Nowadays, metasurface allows building on-chip devices that may efficiently manipulate polarization states. However, it remains challenging to generate different types of polarization states simultaneously, which is required for encoding information for quantum computing and quantum cryptography applications. By introducing geometrical-scaling-induced (GSI) phase modulations, we demonstrate here that an assembly of circularly polarized (CP) and linearly polarized (LP) states can be simultaneously generated by a single metasurface made of L-shaped resonators with different geometrical sizes. Upon illumination, each resonator diffracts CP state with a certain GSI phase. The interaction of these diffractions leads to the desired output beams, where the polarization state and the propagation direction can be accurately tuned by selecting the geometrical shape, size and the spatial sequence of each resonator in the unit cell. This approach resolves a challenging problem in integrated optics and is inspiring for on-chip quantum information processing.

As an intrinsic feature of electromagnetic waves, polarization has facilitated numerous applications in photonics and information technology [1–4]. So far many methods have been employed to modulate the polarization state of light. The most common approach uses optical chirality, where the refractive index differs for the right- and the left-handed circular polarized (RCP and LCP) light [5–7]. Birefringence can also transform the polarization state of the incident light based on different phase velocities of two orthogonal components of the electric field [8]. However, these approaches are volumetric, so the device has to reach certain size in order to tune the polarization state, which is not favorable for integrated photonics. Recently people find that metasurface can effectively manipulate the polarization state of light [9–24]. For circularly polarized (CP) incidence, a rotation-induced geometrical phase, known as Pancharatnam-Berry (P-B) phase, is generated by rotating the anisotropic building elements [25–35]. Yet this phase modulation on LCP and RCP is strongly correlated. For example, when the angular rotation of the element is  $\theta$ , the phase imposed on LCP is  $2\theta$  and that on RCP is  $-2\theta$  [17]. Macroscopically, the beams with the opposite circular polarization are deflected by angles with the same value yet opposite sign if the imposed P-B phase on each building element possesses a linear gradient. If the building elements are arbitrarily selected, the imposed P-B phase does not possess a linear gradient anymore, hence the output beams become either all CP or all linearly polarized (LP). This intrinsic strong correlation of the output states prevents the P-B phase to generate an assembly of polarization states of different types [26, 29].

However, the simultaneous generation of different polarization states is essential for information encoding and quantum cryptography [22, 23, 36, 37]. For example, the paradigm quantum key distribution protocol BB84

employs four from six polarization states (LCP, RCP, horizontal, vertical,  $+45^\circ$ , and  $-45^\circ$  LP, respectively) to constitute two bases [38]. The protocol relies on the quantum property that accessing information is only possible with the cost of disturbing the signal if the dealt states are non-orthogonal, and the non-orthogonal states cannot be cloned [39]. To meet the challenging needs of quantum information, people once proposed a jigsaw puzzle approach and combined six individual spatial regions featured with different P-B phases to generate four LP states and two CP states [30]. However, in addition to the technical issues of the uniformity of output beams and sample size, such a combination approach is not a real sense of integration.

Here we overcome these issues by developing a new strategy to design metasurface, where each element (resonator) of the metasurface diffracts either RCP or LCP state with an additional phase modulation determined by its geometry features. The interaction of these diffractions leads to the desired output beams, where the polarization state and the propagation direction can be accurately controlled by the geometrical shape, size and the spatial sequence of each resonator in the unit cell of the metasurface. In contrast to the rotation-induced P-B phase, here the add-up phase on each resonator depends on its geometrical shape and size, so it is a geometrical-scaling-induced (GSI) phase. We demonstrate that multiple beams with a different type of polarization states can be simultaneously generated from a single metasurface. Let us take L-shaped resonator as an example. The unit cell of the metasurface consists of an assembly of L-shaped resonators with different arm length and width, and their symmetrical isomers (mirror images), as that illustrated in Fig. 1. Depending on the category and sequence of the resonators in the unit cell, left/right-handed CP states ( $|L\rangle/|R\rangle$ ) and horizontally/vertically  $/+45^\circ/-45^\circ$  LP

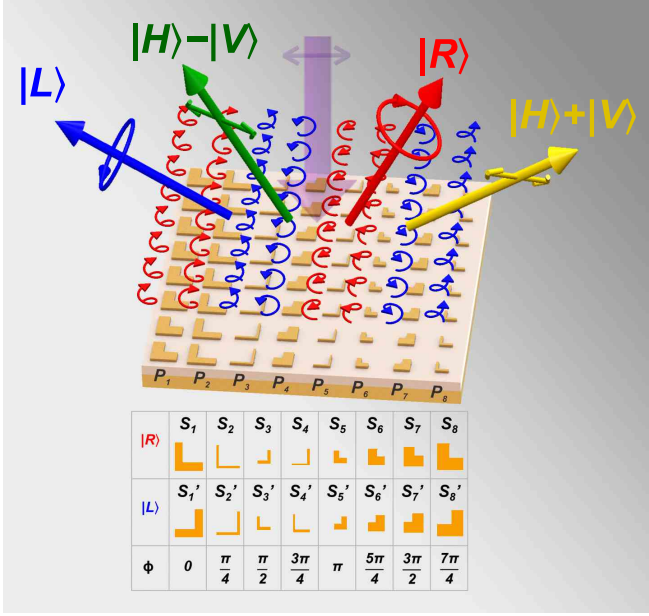


FIG. 1. The schematics showing the generation of multiple coherent beams with different type of polarization states from a metasurface made of L-shaped resonators with different geometrical features. The LP incident beam is represented by the purple arrow. Each L-shaped resonator diffracts a CP state with certain GSI phase  $\phi$ , where the red clockwise arrow represents RCP, and the blue counterclockwise one represents LCP. By controlling the category and the spatial sequence of the L-shaped resonators in the unit cell, the desired CP and/or LP beams (illustrated by the large straight arrows) can be simultaneously generated.

states ( $|H\rangle/|V\rangle/\frac{\sqrt{2}}{2}(|H\rangle + |V\rangle)/\frac{\sqrt{2}}{2}(|H\rangle - |V\rangle)$ ) can be simultaneously generated with any desired combination and propagation direction.

When a plane wave shines on a metasurface made of an array of unit cells ( $N_1 \times N_2$ ), the maxima of the diffraction field  $\vec{E}(k_x, k_y)$  at a distant point S can be expressed as

$$\vec{E}(k_n, k_m) = e^{i(\omega t + \frac{2\pi}{\lambda} r_0)} \cdot N_1 N_2 \cdot \int_{D_x, D_y} \vec{E}(x, y) e^{-i(k_n x + k_m y)} dx dy, \quad (1)$$

where  $\vec{E}(x, y)$  is the electric field over the unit cell,  $k_x$  ( $k_y$ ) is the  $x$ -( $y$ )-component of the wave vector,  $r_0$  is the distance from the center of metasurface to point S,  $D_x$  ( $D_y$ ) is the periodicity of the unit cells in  $x$ -( $y$ )-direction,  $m, n$  are the diffraction orders in  $y$ - and  $x$ -directions, respectively [40]. Details are provided in the Supplementary Materials. Now we consider a unit cell with 8 L-shaped resonators. If the metasurface is so designed that  $D_y < \lambda$  is satisfied, there will be no diffraction in the  $y$ -direction, *i.e.*,  $m$  remains zero. So we can consider the contribution of the resonator assembly in the  $x$ -direction only. Let  $\vec{E}_{P_j}$  denote the diffraction field of each resonator ( $P_j$  with  $j=1, 2, \dots, 8$ ) in the unit cell. It follows that the  $n^{\text{th}}$ -order of the diffraction field

of the metasurface is expressed as

$$\vec{E}(k_n) = e^{i(\omega t + \frac{2\pi}{\lambda} r_0)} N_1 \sum_{j=1}^8 \int_{(j-5)\frac{D_x}{8}}^{(j-4)\frac{D_x}{8}} \vec{E}_{P_j} e^{-i\frac{2\pi n}{D_x} x} dx. \quad (2)$$

To generate multiple beams with desired CP and/or LP states, the amplitude and the phase of the diffracted light from each element in the unit cell should be elaborately designed. It is known that the L-shaped resonator generates CP states by tuning the time retardation ( $\Delta t$ ) between the two arms of the L pattern [10, 11]. Most importantly, depending on the length and width of the arms of L pattern, a specific GSI phase ( $\phi$ ) is imposed on the generated CP state [41]. By taking the mirror image of the L pattern, CP state with the opposite handedness can be generated. Practically, we construct a pool of 16 resonators, 8 resonators make a set  $\{S_i\}$  ( $S_1, S_2, \dots, S_8$ ) generating  $|R\rangle$ ; the other 8 are the mirror structures of  $\{S_i\}$ , forming another set  $\{S'_i\}$  ( $S'_1, S'_2, \dots, S'_8$ ) to generate  $|L\rangle$ , as illustrated in the lower panel of Fig. 1. Upon illumination of an incident beam, GSI phase  $\phi$  is added to each diffraction from the resonators. The range of  $\phi$  for  $\{S_i\}$  is designed to cover 0 to  $2\pi$  with a step of  $\pi/4$ , the same applies for  $\{S'_i\}$ .

To elucidate how the desired state is formed, we first select 8 elements all from  $\{S_i\}$  ( $i=1, 2, \dots, 8$ ). Each element is so arranged spatially that a linear GSI phase gradient is established, as shown in Fig. 2(a). According to Eq. (2), the polarization state of the 1<sup>st</sup> diffraction order is

$$\begin{aligned} \vec{E}(k_1) &= N_1 \sum_{j=1}^8 \int_{(j-5)\frac{D_x}{8}}^{(j-4)\frac{D_x}{8}} \vec{E}_{P_j} e^{-i\frac{2\pi}{D_x} x} dx \\ &= a_1 \sum_{j=1}^8 \vec{E}_{P_j} e^{-i\frac{\pi}{4}(j-4.5)} = 8a_1 e^{i\frac{7\pi}{8}} |R\rangle, \end{aligned} \quad (3)$$

where  $a_1$  is a parameter related to the wavelength and the periodicity in the  $x$ -direction. It is noteworthy that for the scenario of Fig. 2(a),  $n=1$  is the only diffraction beam coming out of the metasurface, which is a pure RCP state. Eq. (2) shows that if  $n$  takes a value other than 1,  $\vec{E}(k_n) = 0$  ( $n \neq 1$ ). When the elements in the unit cell are all taken from  $\{S'_i\}$  in a similar way, *i.e.*,  $S'_8, S'_7, S'_6, \dots, S'_1$ , a pure LCP state is generated, which corresponds to  $-1^{\text{st}}$  order.

Figure 2(b) illustrates a different scenario when the resonators are selected from both  $\{S'_i\}$  and  $\{S_i\}$  as  $S_1, S'_8, S_1, S'_8, S_5, S'_4, S_5, S'_4$ . The corresponding phases and handedness of the diffracted states are  $|R\rangle, e^{i\frac{7\pi}{4}}|L\rangle, |R\rangle, e^{i\frac{7\pi}{4}}|L\rangle, e^{i\pi}|R\rangle, e^{i\frac{3\pi}{4}}|L\rangle, e^{i\pi}|R\rangle, e^{i\frac{3\pi}{4}}|L\rangle$ , respectively.  $n$  satisfies  $|n| \leq \frac{D_x}{\lambda}$  due to the restriction  $|\sin \theta_x| \leq 1$ , where  $\theta_x$  is the diffraction angle. Since the lattice distance in the  $x$ -direction is 700 nm,  $D_x$  becomes 5600 nm. The incident wavelength is chosen as 1300 nm. It follows that  $|n| \leq 4$ . Furthermore, it should be noted that in this structure, once  $n$  is even, the electric field diffracted from the elements  $D_x/2$  apart (*i.e.*,  $P_j$  and  $P_{j+4}$ , with  $j=1, 2, 3, 4$ ) possesses a phase difference of

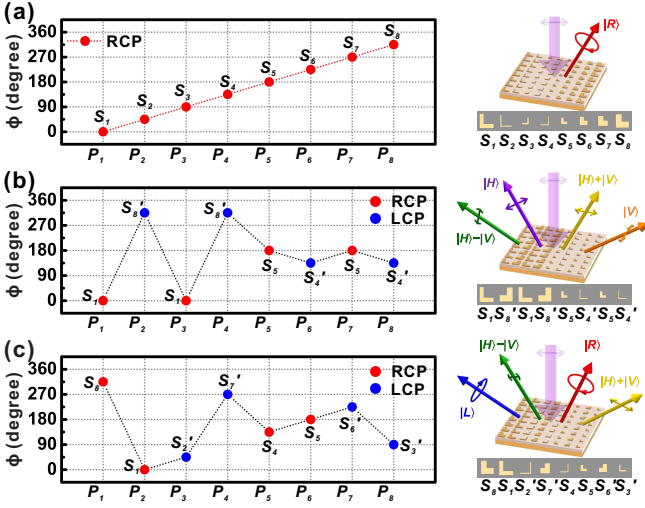


FIG. 2. The plot to show the GSI phase  $\phi$  and the handedness (represented by the red/blue dots) of each resonator in the unit cell. The morphology of the metasurface and the unit cell are illustrated on the right. In the unit cell, the length, width, and symmetry of each resonator vary. (a)  $\phi$  of eight resonators all selected from  $\{S_i\}$  with a linear phase gradient. The output is an RCP state. (b)  $\phi$  of eight resonators, four from  $\{S_i\}$  and four from  $\{S'_i\}$ . The structure generates four LP states. (c)  $\phi$  of another set of 8 resonators selected from  $\{S_i\}$  and  $\{S'_i\}$ , respectively. The output turns out to be two CP and two LP states.

$\pi$ . So their sum-up electric field vanishes. Therefore the observable  $n$  can only be  $\pm 1, \pm 3$ . In Eq. (2), by setting  $n=1$ , the polarization state of the  $1^{st}$  order diffraction is  $\frac{\sqrt{2}}{2}e^{i\frac{3\pi}{8}}(|H\rangle + |V\rangle)$ . By taking  $n=-1, +3, -3$  in Eq. (2), the corresponding polarization states become  $e^{-i\frac{5\pi}{8}}|H\rangle$ ,  $e^{i\frac{3\pi}{8}}|V\rangle$ , and  $\frac{\sqrt{2}}{2}e^{-i\frac{5\pi}{8}}(|H\rangle - |V\rangle)$ , respectively. In this way, four coherent LP states are generated.

By selecting the geometrical shape, size and spatial sequence of each resonator in the unit cell, as well as the lattice distance in the  $x$ -direction, we can obtain any type of polarization state propagating in the desired direction. As illustrated in Fig. 2(c), if the unit cell is made of  $S_8, S_1, S'_2, S'_7, S_4, S_5, S'_6, S'_3$ , the corresponding phase and handedness of the diffraction from these 8 resonators are  $e^{i\frac{7\pi}{4}}|R\rangle, |R\rangle, e^{i\frac{\pi}{4}}|L\rangle, e^{i\frac{6\pi}{4}}|L\rangle, e^{i\frac{3\pi}{4}}|R\rangle, e^{i\pi}|R\rangle, e^{i\frac{5\pi}{4}}|L\rangle, e^{i\frac{2\pi}{4}}|L\rangle$ , respectively. For the aforementioned reason,  $n$  can only be  $\pm 1$  and  $\pm 3$ . It follows that corresponding to  $n=3, 1, -1, -3$ , the polarization states become  $\frac{\sqrt{2}}{2}e^{-i\frac{5\pi}{8}}(|H\rangle + |V\rangle), e^{i\frac{5\pi}{8}}|R\rangle, \frac{\sqrt{2}}{2}e^{-i\frac{1\pi}{8}}(|H\rangle - |V\rangle)$ , and  $e^{i\frac{9\pi}{8}}|L\rangle$ , respectively. This means that two CP (LCP, RCP) states and two LP ( $+45^\circ, -45^\circ$ ) states with fixed phase difference are simultaneously generated.

To experimentally verify our design shown in Figs. 2(b)-2(c), we fabricate the arrays of L-shaped resonator assembly, as shown in Fig. 3(a) and Fig. 4(a), respectively. A supercontinuum laser and a Glan-Taylor polarizer are used to generate the LP incident beam. The propagation direction of each diffraction beam satisfies

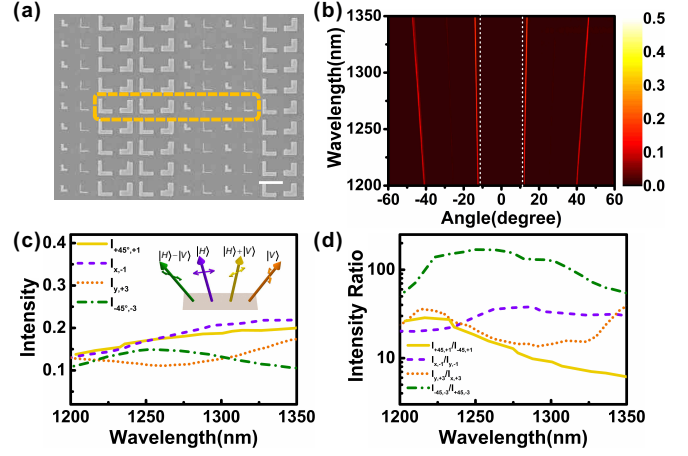


FIG. 3. (a) SEM micrograph of the fabricated metasurface as designed in Fig. 2(b). The unit cell is marked by the dash line box. The bar represents  $1 \mu\text{m}$ . (b) Measured angular-resolved diffraction spectra. Four bright lines represent the diffracted beams measured at a different wavelength at different diffraction angles. The color bar stands for the intensity. (c) The normalized beam intensity of four diffracted beams.  $I_{+45^\circ, +1}$  represents the intensity of  $+1^{st}$  order of an LP state with  $45^\circ$ -polarization.  $I_{x, -1}$  represents the intensity of  $-1^{st}$  order of an  $x$ -polarized state.  $I_{y, +3}$  represents the intensity of  $+3^{rd}$  order of a  $y$ -polarized state.  $I_{-45^\circ, -3}$  represents the intensity of  $-3^{rd}$  order of an LP state with  $-45^\circ$ -polarization. (d) The measured light intensity ratio of each beam, which is defined as the intensity of the measured beam divided by the intensity of its conjugated beam.  $I_{+45^\circ, +1}/I_{-45^\circ, +1}$  represents the ratio for the beam with  $45^\circ$ -polarization ( $+1^{st}$  order).  $I_{x, -1}/I_{y, -1}$  represents the ratio for the  $x$ -polarized state ( $-1^{st}$  order).  $I_{y, +3}/I_{x, +3}$  represents the ratio for the beam with the  $y$ -polarized state ( $+3^{rd}$  order).  $I_{-45^\circ, -3}/I_{+45^\circ, -3}$  represents the ratio for the beam with  $-45^\circ$ -polarization ( $-3^{rd}$  order).

$\sin \theta_x = \frac{n}{D_x} \lambda$ . An angular-resolved detector measures the diffraction intensity. To identify the polarization state of each diffracted beam, an achromatic quarter wave plate and/or a polarizer are installed in front of the detector (see Supplementary Material for details). The angle-resolved diffraction spectra are illustrated in Fig. 3(b) and Fig. 4(b), where the detection angle covers from  $-60^\circ$  to  $-12^\circ$  and  $12^\circ$  to  $60^\circ$ . The region between the white dash lines cannot be detected due to the technical restriction of the reflection mode. Experimentally we define a parameter, the light intensity ratio, to characterize the purity of each generated state. For the LP beam, the light intensity ratio is defined as the ratio of the intensity of the investigated beam and the intensity detected with the orthogonal polarization; For the CP beam, it is defined as the ratio of the intensity of the investigated beam and that with the conjugated CP. Theoretically, this ratio should be infinity for pure CP/LP state. Yet experimentally the conjugated polarization state does not vanish completely. So this ratio usually ends up with a large value. The large ratio suggests that each resonator in the unit cell contributes

more accurate phase and amplitude, so the interaction of all the diffracted light leads to the beams with the desired polarization states.

For the sample shown in Fig. 3(a), four diffraction beams, from left to right, correspond to  $3^{rd}$ ,  $1^{st}$ ,  $-1^{st}$ , and  $-3^{rd}$  order of diffraction (Fig. 3(b)). To characterize the diffraction efficiency, we define the normalized beam intensity as the ratio of the intensity of the diffracted beam and that of the incident beam, as shown in Fig. 3(c). In the wavelength range of 1200-1350 nm, the normalized intensity of each diffraction beam is higher than 10%, and the total normalized intensity of diffraction beams is higher than 50%. In particular, at 1300 nm the intensity of each diffraction order is higher than 12% and the total normalized diffraction intensity reaches 65%. Figure 3(d) shows the light intensity ratio of the four beams. It can be seen that the intensity ratio of each beam is larger than 10 for the wavelength between 1200 nm to 1275 nm, and the maximum reaches 168 at 1260 nm. Figure 3D confirms that the polarization states of the output beams are in agreement with theoretical expectations.

To generate two CP and two LP beams, we fabricate the structures shown in Fig. 2(c). The SEM micrograph of the structure is presented in Fig. 4(a), one can identify that the resonators in the unit cell are  $S_8$ ,  $S_1$ ,  $S'_2$ ,  $S'_4$ ,  $S_5$ ,  $S'_6$ ,  $S'_3$ , respectively. Fig. 4(b) indicates that four diffraction beams are simultaneously generated, and the normalized beam intensity is shown in Fig. 4(c). Within the wavelength range of 1200-1325 nm, the normalized intensity of each diffracted beam is higher than 8%, and the total normalized intensity in these four directions is larger than 58%. At 1275 nm, the intensity of each diffraction beam is higher than 16%, and the total normalized intensity reaches 68%. The light intensity ratio of these four beams is presented in Fig. 4(d), which is always higher than 10 in the wavelength range 1210-1300 nm, and the maximum reaches 76 at 1225 nm. Figure 4(d) confirms that two CP states and two LP states have indeed been experimentally realized.

We should emphasize that the number of diffraction beams and the propagation direction of these beams can be accurately modulated. The number of the diffraction beams is decided essentially by the diffraction order  $n$ , which depends on the ratio of the periodicity of the unit cell in the  $x$ -direction  $D_x$  and the wavelength  $\lambda$ . The propagation direction of each light beam is associated with the diffraction order. As we discussed earlier,  $n$  satisfies  $|n| \leq \frac{D_x}{\lambda}$ . For the scenario  $3\lambda < D_x < 5\lambda$ ,  $n = \pm 1, \pm 3$  can be diffracted from the metasurface to four different directions (Figs. 3-4). However, if  $\lambda < D_x < 3\lambda$ ,  $|n| < 3$ . This means that only two beams with  $\pm 1^{st}$  diffraction order can be generated. Therefore, by tuning  $D_x/\lambda$ , the number of diffraction beams and the diffraction orientation of each beam can be controlled.

Once the resonators in the unit cell have been selected, the sequence of these resonators determines which

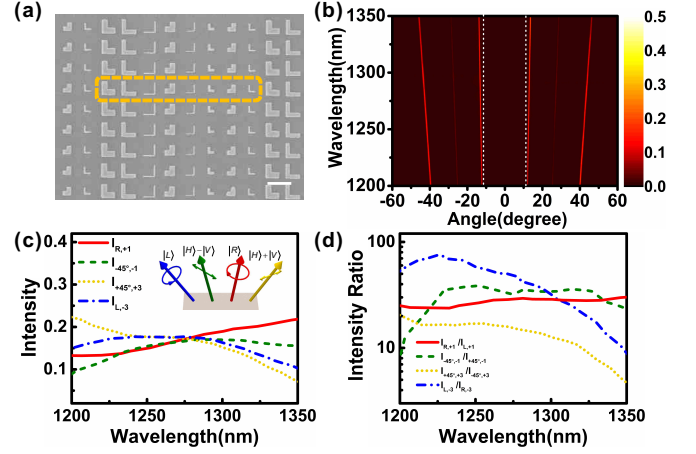


FIG. 4. (a) SEM micrograph of the fabricated metasurface as designed in Fig. 2(c). The unit cell is marked by the dash line box. The bar stands for  $1 \mu\text{m}$ . (b) Measured angular-resolved diffraction spectra. Four bright lines represent the diffracted beams measured at a different wavelength at different diffractive angles. The color bar stands for the intensity. (c) The normalized beam intensity of four diffracted beams.  $I_{R,+1}$  represents the intensity of the  $+1^{st}$  order of an RCP state.  $I_{L,-45^\circ,-1}$  represents the intensity of a  $-45^\circ$ -polarized LP state.  $I_{+45^\circ,+3}$  represents the intensity of  $+3^{rd}$  order of a  $45^\circ$ -polarized LP state.  $I_{L,-3}$  represents the intensity of  $-3^{rd}$  order of an LCP state. (d) The measured light intensity ratio of each diffracted beam, which is defined as the intensity of the measured beam divided by the intensity of its conjugated beam.  $I_{R,+1}/I_{L,+1}$  represents the ratio for the RCP state ( $+1^{st}$  order).  $I_{L,-45^\circ,-1}/I_{+45^\circ,-1}$  represents the ratio for the  $-45^\circ$ -polarized LP ( $-1^{st}$  order).  $I_{+45^\circ,+1}/I_{-45^\circ,+3}$  represents the ratio for the  $45^\circ$ -polarized LP ( $+3^{rd}$  order).  $I_{L,-3}/I_{R,-3}$  represents the ratio for the LCP state ( $-3^{rd}$  order).

polarization state comes out from certain diffraction order. Let us take the unit cell ( $S_8$ ,  $S_1$ ,  $S'_2$ ,  $S'_4$ ,  $S_5$ ,  $S'_6$ ,  $S'_3$ ) as an example, which contains the same group of resonators as that shown in Fig. 4(a). The assembly of these resonators has totally  $40320 (A_8^8)$  combination scenarios. Considering the scenario that the electric field diffracted from the elements  $D_x/2$  apart (*i.e.*,  $P_j$  and  $P_{j+4}$ , with  $j=1, 2, 3, 4$ ) possesses a phase difference of  $\pi$ , the sum-up electric field of even and the  $0^{th}$  diffraction order vanishes. Therefore, the observable diffraction order  $n$  can only be  $\pm 1, \pm 3$ , and the number of combinations is accordingly reduced to  $384 (C_8^1 C_6^1 C_4^1 C_2^2)$ . Furthermore, the output states will remain unchanged if the assembly of the resonators possesses translational symmetry in the periodic structure in the  $x$ -direction. It follows that the number of the independent assembly is further reduced from 384 to 48. 8 of 48 combinations can generate two CP (LCP, RCP) states and two LP ( $+45^\circ$ ,  $-45^\circ$ ) states. For example, if the sequence is rearranged as  $S_4$ ,  $S_1$ ,  $S'_2$ ,  $S'_3$ ,  $S_8$ ,  $S_5$ ,  $S'_6$ ,  $S'_7$ , the output states will be RCP,  $-45^\circ$ -LP, LCP, and  $+45^\circ$ -LP, corresponding to the diffraction order -3, -1, +1, and +3, respectively. If,

however, the sequence becomes  $S_8, S_1, S'_6, S'_3, S_4, S_5, S'_2, S'_7$ , the output states turn out to be LCP,  $+45^\circ$ -LP, RCP, and  $-45^\circ$ -LP instead. More examples are provided in Table S3 in Supplementary Materials.

Encoding, transmission, and processing of information are important issues in quantum information science [42, 43]. As the basic unit of quantum information processing, qubit gate can be constructed with polarizing beam splitters, phase shifters, and waveplates, *etc.*, which are bulky and heavy if the conventional optical devices are applied [43]. Developing new principle optical devices on the micro/nanoscale is essential for future integrated photonics and information technology. The approach demonstrated in this report provides a promising solution, which allows simultaneous generating arbitrary combination of CP and LP states. By judiciously selecting the geometrical size and the symmetry of each resonator in the unit cell and by carefully designing the lattice parameter, we are able to accurately control the output polarization states, the number of output beams, and the propagation direction of each beam. In contrast to the P-B phase modulation, which either generates pairs of RCP and LCP states, or LP states with the same polarization, our approach breaks the limitation and correlation on the type of polarization states in the output beams. This approach provides new perspectives in generating an arbitrary assembly of polarization states with high integration and hence is enlightening in constructing quantum states [23], realizing quantum entanglement [22] and qubit gates [42], and developing quantum cryptography [36, 38].

This work was supported by the projects from the National Key R&D Program of China (2017YFA0303702), and from the National Natural Science Foundation of China (11634005, 11674155, 11574141, 11621091 and 11704179), and from Jiangsu Province (Grant No. BK20160065).

---

\* Corresponding author: rwpeng@nju.edu.cn

† Corresponding author: muwang@nju.edu.cn

- [1] X. Yin, Z. Ye, J. Rho, Y. Wang, and X. Zhang, *Science* **339**, 1405 (2013).
- [2] M. Scheucher, A. Hilico, E. Will, J. Volz, and A. Rauschenbeutel, *Science* **354**, 1577 (2016).
- [3] S.-H. Gong, F. Alpeggiani, B. Sciacca, E. C. Garnett, and L. Kuipers, *Science* **359**, 443 (2018).
- [4] H. Zhou, C. Peng, Y. Yoon, C. W. Hsu, K. A. Nelson, L. Fu, J. D. Joannopoulos, M. Soljačić, and B. Zhen, *Science* **359**, 1009 (2018).
- [5] J. K. Gansel, M. Thiel, M. S. Rill, M. Decker, K. Bade, V. Saile, G. von Freymann, S. Linden, and M. Wegener, *Science* **325**, 1513 (2009).
- [6] C. Pfeiffer, C. Zhang, V. Ray, L. J. Guo, and A. Grbic, *Phys. Rev. Lett.* **113**, 023902 (2014).
- [7] T.-T. Kim, S. S. Oh, H.-D. Kim, H. S. Park, O. Hess, B. Min, and S. Zhang, *Sci. Adv.* **3**, e1701377 (2017).
- [8] M. Born and E. Wolf, *Principles of Optics* (Cambridge University Press, 1999).
- [9] N. Yu, P. Genevet, M. A. Kats, F. Aieta, J.-P. Tetienne, F. Capasso and Z. Gaburro, *Science* **334**, 333 (2011).
- [10] S.-C. Jiang, X. Xiong, P. Sarriugarte, S.-W. Jiang, X.-B. Yin, Y. Wang, R.-W. Peng, D. Wu, R. Hillenbrand, X. Zhang, and M. Wang, *Phys. Rev. B* **88**, 161104(R) (2013).
- [11] S.-C. Jiang, X. Xiong, Y.-S. Hu, Y.-H. Hu, G.-B. Ma, R.-W. Peng, C. Sun, and M. Wang, *Phys. Rev. X* **4**, 021026 (2014).
- [12] X. Xiong, Y.-S. Hu, S.-C. Jiang, Y.-H. Hu, R.-H. Fan, G.-B. Ma, D.-J. Shu, R.-W. Peng, and M. Wang, *Appl. Phys. Lett.* **105**, 201105 (2014).
- [13] R.-H. Fan, Y. Zhou, X.-P. Ren, R.-W. Peng, S.-C. Jiang, D.-H. Xu, X. Xiong, X.-R. Huang, and M. Wang, *Adv. Mater.* **27**, 1201 (2015).
- [14] A. Arbabi, Y. Horie, M. Bagheri, and A. Faron, *Nat. Nanotechnol.* **10**, 937 (2015).
- [15] Z.-H. Wang, S.-C. Jiang, X. Xiong, R.-W. Peng, and M. Wang, *Appl. Phys. Lett.* **108**, 261107 (2016).
- [16] D. Pan, H. Wei, L. Gao, and H. Xu, *Phys. Rev. Lett.* **117**, 166803 (2016).
- [17] J. P. Balthasar Mueller, N. A. Rubin, R. C. Devlin, B. Groever, and F. Capasso, *Phys. Rev. Lett.* **118**, 113901 (2017).
- [18] R. C. Devlin, A. Ambrosio, N. A. Rubin, J. P. Balthasar Mueller, and F. Capasso, *Science* **358**, 896 (2017).
- [19] P. C. Wu, J.-W. Chen, C.-W. Yin, Y.-C. Lai, T. L. Chung, C. Y. Liao, B. H. Chen, K.-W. Lee, C.-J. Chuang, C.-M. Wang, and D. P. Tsai, *ACS Photonics* **5**, 2568 (2017).
- [20] J. Li, S. Kamin, G. Zheng, F. Neubrech, S. Zhang, and N. Liu, *Sci. Adv.* **4**, eaar6768 (2018).
- [21] N. A. Rubin, A. Zaidi, M. Juhl, R. P. Li, J. P. Balthasar Mueller, R. C. Devlin, K. Lesson, and F. Capasso, *Opt. Express* **26**, 21455 (2018).
- [22] T. Stav, A. Faerman, E. Maguid, D. Oren, V. Kleiner, E. Hasman, and M. Segev, *Science* **361**, 1101 (2018).
- [23] K. Wang, J. G. Titchener, S. S. Kruk, L. Xu, H.-P. Chung, M. Parry, I. I. Kravchenko, Y.-H. Chen, A. S. Solntsev, Y. S. Kivshar, D. N. Neshev, and A. A. Sukhorukov, *Science* **361**, 1104 (2018).
- [24] A. D.-Rubio, J. Li, C. Shen, S. A. Cummer, and S. A. Tretyakov, *Sci. Adv.* **5**, eaau7288 (2019).
- [25] G. Zheng, H. Mühlenbernd, M. Kenney, G. Li, T. Zentgraf, and S. Zhang, *Nat. Nanotechnol.* **10**, 308 (2015).
- [26] A. Shaltout, J. Liu, A. Kildishev, and V. Shalaev, *Optica* **2**, 860 (2015).
- [27] M. Tymchenko, J. S. G.-Diaz, J. Lee, N. Nookala, M. A. Belkin, and A. Alù, *Phys. Rev. Lett.* **115**, 207403 (2015).
- [28] M. Khorasaninejad, W. T. Chen, R. C. Devlin, J. Oh, A. Y. Zhu, and F. Capasso, *Science* **352**, 1190 (2016).
- [29] D. Wen, F. Yue, C. Zhang, X. Zang, H. Liu, W. Wang, and X. Chen, *Appl. Phys. Lett.* **111**, 023102 (2017).
- [30] P. C. Wu, W.-Y. Tsai, W. T. Chen, Y.-W. Huang, T.-Y. Chen, J.-W. Chen, C. Y. Liao, C. H. Chu, G. Sun, and D. P. Tsai, *Nano Lett.* **17**, 445 (2017).
- [31] W. T. Chen, A. Y. Zhu, V. Sanjeev, M. Khorasaninejad, Z. Shi, E. Lee, and F. Capasso, *Nat. Nanotechnol.* **13**, 220 (2018).
- [32] S. Wang, P. C. Wu, V.-C. Su, Y.-C. Lai, M.-K. Chen, H. Y. Kuo, B. H. Chen, Y. H. Chen, T.-T. Huang, J.-H. Wang, R.-M. Lin, C.-H. Kuan, T. Li, Z. Wang, S. Zhu,

- and D. P. Tsai, Nat. Nanotechnol. **13**, 227 (2018).
- [33] F. Zhong, J. Li, H. Liu, and S. Zhu, Phys. Rev. Lett. **120**, 243901 (2018).
  - [34] N. Shitrit, J. Kim, D. S. Barth, H. Ramezani, Y. Wang, and X. Zhang, Phys. Rev. Lett. **121**, 046101 (2018).
  - [35] P. K. Jha, N. Shitrit, X. Ren, Y. Wang, and X. Zhang, Phys. Rev. Lett. **121**, 116102 (2018).
  - [36] Z. Tang, Z. Liao, F. Xu, B. Qi, L. Qian, and H.-K. Lo, Phys. Rev. Lett. **112**, 190503 (2014).
  - [37] H. Takenaka, A. C.-Casado, M. Fujiwara, M. Kitamura, M. Sasaki, and M. Toyoshima, Nat. Photon. **11**, 502 (2017).
  - [38] N. Gisin, G. Ribordy, W. Tittel, and H. Zbinden, Rev. Mod. Phys. **74**, 145 (2002).
  - [39] P. Meystre and M. Sargent, *Elements of Quantum Optics* (Springer, 2007).
  - [40] E. Hecht, *Optics* (Pearson Education Ltd., 2013).
  - [41] See Supplementary Material for further theoretical and experimental detail.
  - [42] J. L. O'Brien, Science **318**, 1567 (2007).
  - [43] D. Tiarks, S. S.-Eberle, T. Stolz, G. Rempe, and S. Dürr, Nat. Phys. **15**, 124 (2019).